MIMO Based Decoupling Strategy for Grid Connected Power Converters Controlled in the Synchronous Reference Frame

Javier Samanes, Eugenio Gubia and Jesus Lopez
Electrical, Electronic and Communication Engineering, Institute of Smart Cities
Public University of Navarre
Pamplona, Spain
javier.samanes@unavarra.es

***Abstract*—Power converters are frequently connected to the grid through a *LCL* filter, controlling its power transfer through a current control loop in the synchronous reference frame. In this reference frame, cross coupling terms appear between the current and voltages of the passive components, which, without a proper decoupling strategy, penalize the converter transient response and the current control adjustment. In this work, an intuitive decoupling strategy is presented to improve the dynamic behavior, based on Multiple-Input-Multiple-Output systems theory. The approach developed is particularly interesting in extremely weak grids, allowing an easier adjustment of the main controller.**

***Index Terms*—Converter current control, *LCL*-filter, synchronous reference frame, decoupling.**

I. Introduction

Grid-connected power converters are commonly used for power quality management in renewable energy generation systems. In such systems the voltage source converter (VSC) is an extended solution, having a *LCL* filter to attenuate the switching harmonics and meet the current standards for grid connection [1]. *LCL* type filters are used because they offer strong attenuation, while presenting a compromise between filter simplicity and reduced size and cost [2].

To properly control the power transferred to the grid, a current control mode is normally the preferred option. Such controller can be implemented either in a stationary frame, or in a rotating (also called synchronous) reference frame (SRF), being the latest the scope of this work. The SRF approach offers the possibility of controlling the current, with zero tracking error, by means of a common proportional-integral (PI) controller, as the fundamental frequency component, is transformed to a DC component. This transformation has a main drawback; as it is known, cross-coupling terms appear between the quadrature axis, denoted as *dq*, of the SRF model of the *LCL* filter. To simplify the controller design procedure and improve its dynamic response, decoupling strategies have been widely used, and can be classified into two main groups, namely, state-feedback decoupling (SFD) [3]–[5], using generally the converter current feedback, and feed-forward decoupling such as complex vector decoupling (CVD) [6], [7], MIMO controller design [8] and current reference feed-forward [9].

The state feedback decoupling is the dominant approach in the literature, but its performance is poorer when it is applied to converters connected to weak grids. Moreover, it can be highly affected by the existing delays in the feedback path, such as filters and computation. The complex vector decoupling approach is based on the design of a complex PI that cancels the plant cross couplings, but the parameters of the PI are set as a function of the plant, conditioning the achievable dynamics [9]. In this work, an intuitive decoupling feed-forward approach is developed based on a MIMO cross-controller-decoupler (CCD), that simplifies the design of the current controller. Robustness face to plant uncertainties such as grid inductance variations and parameter tolerances are tested. The grid disturbance rejection is also evaluated.

This work has been supported by the Spanish State Research Agency (AEI) and FEDER-UE under grant DPI2016-80641-R, and partially funded by the Public University of Navarre through a doctoral scholarship.

II. Fundamentals of the Cross Controller Decoupler

The decoupling strategy can be intuitively derived for a purely inductive filter and supposing a controller with no delays. Once the MIMO cross controller decoupler is derived for the simplified system, it is extended to a *LCL* filter in Section III, considering the control delays and measurement filters.

When the SRF model is obtained for an inductance, cross coupling terms between both *dq* phases appear, as indicated by Fig. 1. Its dynamics are given by Eq. 1, where $G_1(s)$ and $G_2(s)$ are given by Eq. 2 and Eq. 3 respectively, with L_c the inductance value, R_c its series equivalent resistance and ω_0 the angular velocity of the rotating reference frame.

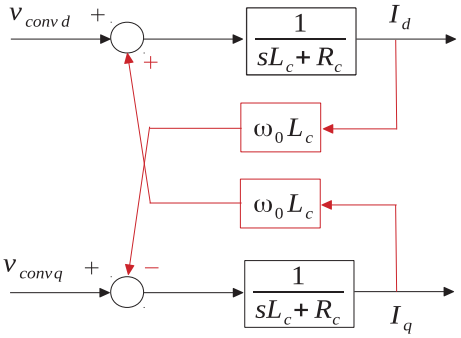

Fig. 1. Inductance model in SRF.

$$\begin{bmatrix} I_d(s) \\ I_q(s) \end{bmatrix} = \begin{bmatrix} G_1(s) & G_2(s) \\ -G_2(s) & G_1(s) \end{bmatrix} \begin{bmatrix} V_{convd}(s) \\ V_{convq}(s) \end{bmatrix} \quad (1)$$

$$G_1(s) = \frac{L_c s + R_c}{(L_c s + R_c)^2 + (\omega_0 L_c)^2} \quad (2)$$

$$G_2(s) = \frac{\omega_0 L_c}{(L_c s + R_c)^2 + (\omega_0 L_c)^2} \quad (3)$$

To achieve a diagonal system in Eq. 1, the feedback of the inductance current can be used as indicated in Fig. 2 by the dashed blue lines, multiplying the current by the cross term $\omega_0 L_c$. This decoupling technique is called SFD, and if the inductance is known it can achieve a perfect decoupling, as shown in Fig. 3. In this figure the inductance model in the SRF is represented in blue, where $G_2(s)$ has a greater magnitude at low frequencies than $G_1(s)$. With the SFD, in red, $G_2(s)$ is eliminated and the frequency response of a pure decoupled inductance is obtained.

Another alternative strategy to achieve a decoupled inductor is the application of two cross-decoupler transfer functions, $CD_1(s)$ and $CD_2(s)$, to the controller voltage $v_{cont\ dq}$ as indicated in Fig. 2 by the blue continuous lines. $CD_1(s)$ and $CD_2(s)$ must cancel the cross coupling effect, something that

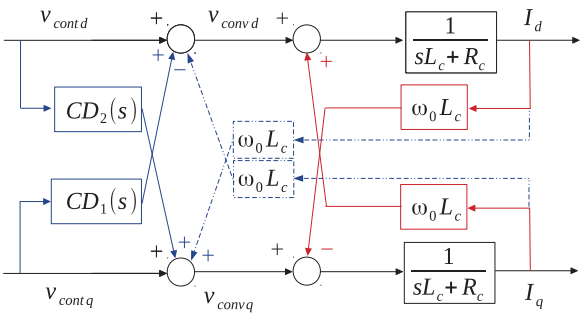

Fig. 2. Inductance model and CCD in continuous blue lines and SFD in dashed blue lines.

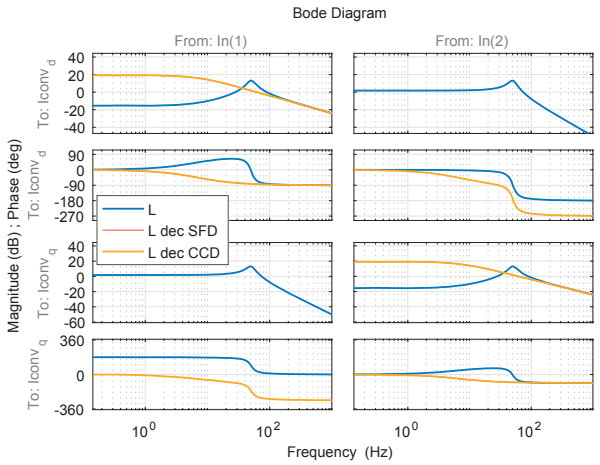

Fig. 3. Bode representation of the inductance modeled in the SRF (blue), decoupled with SFD (red) and decoupled with the CCD (yellow).

can be achieved by selecting $CD_1(s) = -G_2(s)/G_1(s)$ and $CD_2(s) = G_2(s)/G_1(s)$. The CCD, $CD_1(s)$, for an inductor is given by the simple expression in Eq. 4.

$$CD_1(s) = -\frac{\omega_0 L_e}{L_e s + R_e} \quad (4)$$

The decoupling term is a decoupled inductor, L_e with a series resistance R_e and a gain dependent on the inductance and the angular velocity of the SRF. If these parameters match the plant ones, a perfect decoupling is achieved, as it is represented in Fig. 3, where again, $G_2(s)$ is eliminated, and the frequency response of a decoupled inductor is obtained.

The application of the proposed CCD decoupling strategy is presented in the next section for a power converter with a *LCL* filter at the output, the standard solution for grid-connected VSC.

III. Decoupling Strategy for a *LCL* Filter

A. System Description and Modeling

Fig. 4 shows the scheme of a power converter with a *LCL* filter connected to the grid and its control structure. This topology is typically used as an interface for renewable energy generating system, where the DC link is connected to a PV array or the machine side converter of a wind turbine. In this figure, L_c stands for the converter inductance, C_f for the filter capacitor, L_{transf} for the transformer leakage inductance and L_g for the effective grid inductance, which varies depending on the grid at which the power converter is connected and the power injected at the coupling point [10].

The capacitor line voltage, U_{Cf}, and the converter side current, I_{conv}, are measured and filtered by a low pass first order analog filter with a cut-off frequency of 1 kHz, *LPAF(s)*, in order to attenuate the switching harmonics. The filtered measurements are fed to the digital signal processor (DSP), where the control algorithm is executed once per switching frequency, what is called symmetrical sampling. The PLL

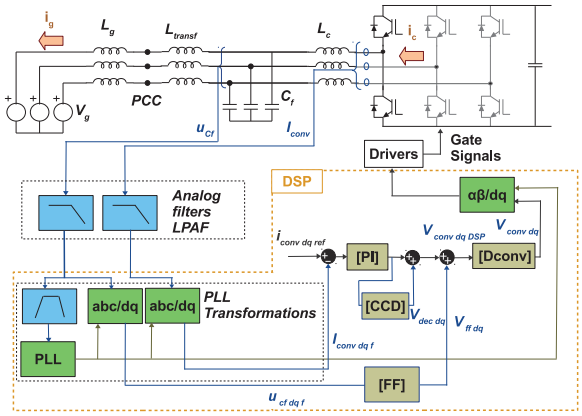

Fig. 4. VSC connected to the grid and its control structure with the proposed compensation [CCD] and [FF].

receives the capacitor voltage through a SOGI filter and provides the angle for the transformation to the SRF. The current measured is also transformed to the SRF frame, where a proportional integral (PI) controller is responsible of providing the required action for zero-tracking error in both dq axis. In Fig. 4 the PI controller is represented by [PI] to denote that it is a matrix, diagonal in this case. The capacitor voltage measurements, expressed in the SRF $U_{Cf\ dq}$ are summed to the PI controller action through a matrix [FF], the purpose of this matrix is explained in the next subsection. At last, the [CCD] matrix is the proposed decoupling strategy for *LCL* filters, which is presented in the following.

As a result of the transformation to the SRF of the *LCL* filter variables, in order to control the current with a PI controller, cross-coupling terms appear between the reactive passive components of the plant, as illustrated by Fig. 5. The system is modeled as a MIMO system taking into account such cross-couplings. To analyze the system stability all the elements are modeled in the same reference system. For this reason, the low pass analog filters (LPAF(s)) and the approximation for the computation delay and ZOH [11] (Dconv(s)), defined in $\alpha\beta$, are transformed to dq using the theory in [12]. In this way two matrices are obtained [LPAF(s)], given by Eq. 5 and [Dconv(s)] given by Eq. 6.

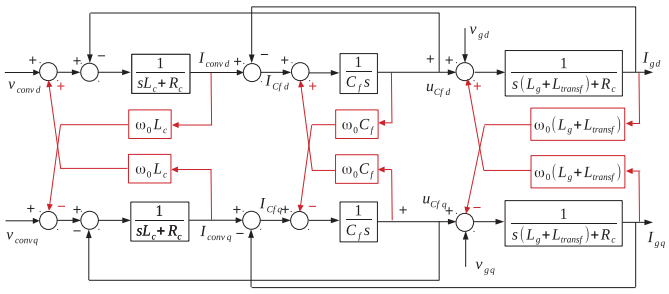

Fig. 5. SRF model of the LCL system.

$$[LPAF(s)] = \begin{bmatrix} LPAF_1(s) & LPAF_2(s) \\ -LPAF_2(s) & LPAF_1(s) \end{bmatrix} \quad (5)$$

$$[D_{conv}(s)] = \begin{bmatrix} D_1(s) & D_2(s) \\ -D_2(s) & D_1(s) \end{bmatrix} \quad (6)$$

The diagonal terms of the matrix [LPAF(s)] in dq are $LPAF_1(s) = LPAF(s + j\omega_0) + LPAF(s - j\omega_0)$ and the anti-diagonal terms are $LPAF_2(s) = (jLPAF(s + j\omega_0) - jLPAF(s - j\omega_0))$ [12]. The same transformation is used to obtain the terms in Eq. 6.

B. Decoupler Adjustment and Controller Design

In Section II the CCD was adjusted to cancel the cross coupling terms, something that cannot be achieved for a grid connected power converter without an accurate estimation of L_g. Moreover, the MIMO model for the *LCL* is a sixth order model, so the complexity of the CCD transfer function is highly increased, even if an accurate estimation of the grid inductance is obtained.

The capacitor voltage feed-forward, shown in Fig. 4, increases the rejection to perturbations in the grid, but it also helps to immunize the system face to grid inductance variations. This voltage feed-forward can effectively cancel the variability in the control loop created by the unknown and variable grid impedance if the delays in the control loop are eliminated or compensated [13]. However, this cannot always be acheived, and the delays introduced by the measurement filters (LPAF), computation and ZOH (D_{conv}) deteriorates the effect of the capacitor voltage feed-forward. To alleviate these effects the matrix [FF] is added in the voltage feed-forward in the diagram of Fig. 4. Fig. 4 can be represented as a block diagram, obtaining Fig. 6.

From Fig. 6 it is clear that the voltage feed-forward is affected by the product of [LPAF], [FF] and $[D_{conv}]$. If [FF] is considered to be the identity matrix the product of the three matrices is represented in Eq. 7 in terms of $A(s)$ and $B(s)$. This equation correlates the capacitor voltage in the SRF, $U_{Cf\ dq}$, and the voltage feed-forward action $V_{dq\ FF}$, where $A(s) = D_1(s)LPAF_1(s) - D_2(s)LPAF_2(s)$ and $B(s) = D_1(s)LPAF_2(s) + D_2(s)LPAF_1(s)$.

$$\begin{bmatrix} V_{dFF}(s) \\ V_{qFF}(s) \end{bmatrix} = \begin{bmatrix} A(s) & B(s) \\ -B(s) & A(s) \end{bmatrix} \begin{bmatrix} U_{Cfd}(s) \\ U_{Cfq}(s) \end{bmatrix} \quad (7)$$

Eq. 7 reveals that the voltage feed-forward in the d axis, $V_{d\ FF}$, contains both measurements $U_{Cf\ d}$ and $U_{Cf\ q}$. The same coupling is obtained in the q axis. In order to avoid the cross couplings in the voltage feed-forward, a compensation is required in [FF]. By imposing that $V_{dFF}(s) = U_{Cfd}(s)$ and $V_{qFF}(s) = U_{Cfq}(s)$ the compensation terms required to eliminate the effects of $[D_{conv}]$ and [LPAF] are obtained, which are given in Eq. 8.

$$[FF] = \begin{bmatrix} \frac{A(s)}{A(s)^2+B(s)^2} & -\frac{B(s)}{A(s)^2+B(s)^2} \\ \frac{B(s)}{A(s)^2+B(s)^2} & \frac{A(s)}{A(s)^2+B(s)^2} \end{bmatrix} \quad (8)$$

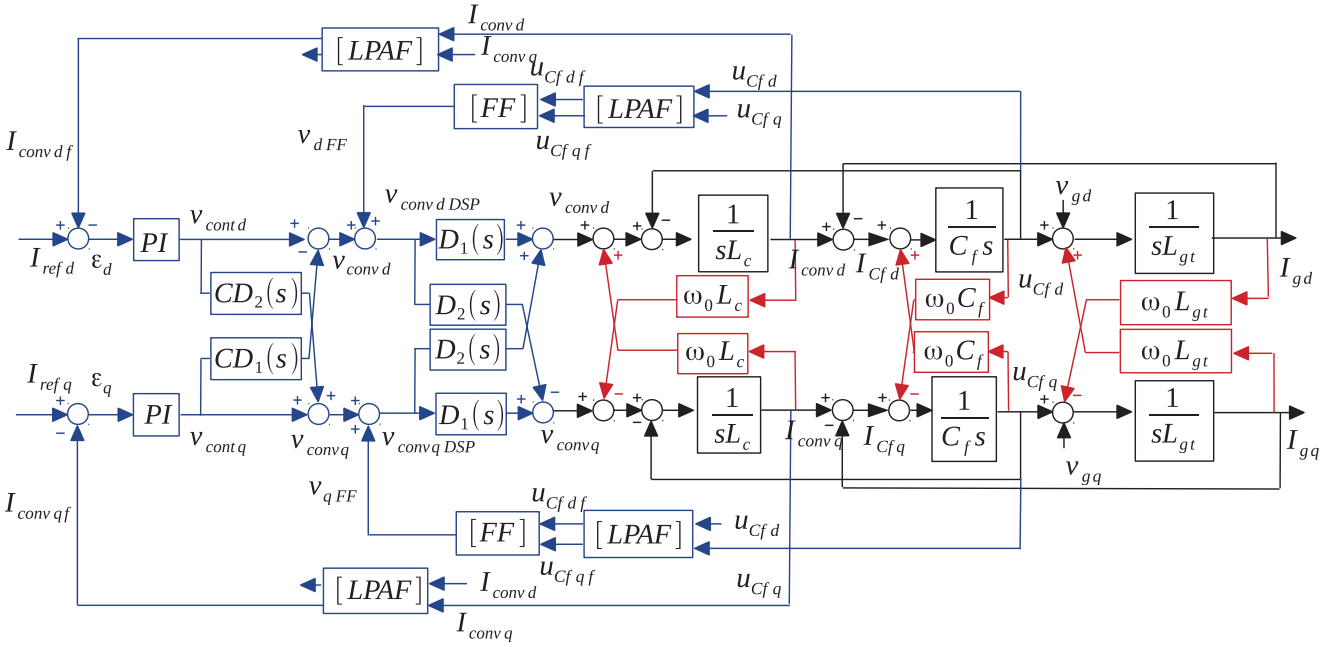

Fig. 6. VSC connected to the grid and its control structure with the proposed compensation.

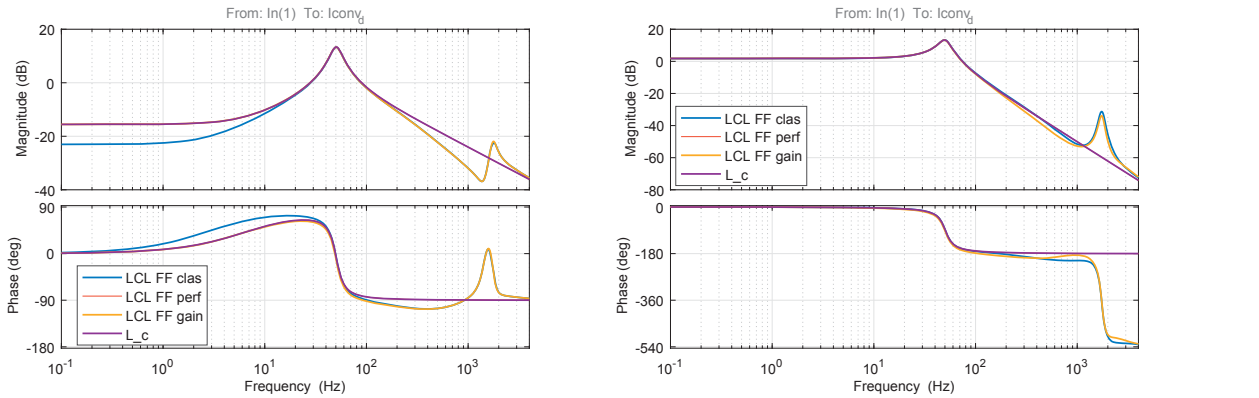

Fig. 7. Frequency response of the converter current, I_{conv_d}, with respect to the converter voltage $V_{conv\ d}$ (left) and $V_{conv\ q}$ (right) for different FF options: classical (blue), perfect (red), gain approximation (yellow) and a pure inductance (purple).

In Fig. 7 the bode plot of I_{conv_d} with respect to $V_{conv\ d}$ and $V_{conv\ q}$ is plotted for different voltage feed-forwards and a pure inductance. As the system is symmetric, only the diagonal element, representing the converter current in an axis created by a voltage in the same axis, and the anti-diagonal, representing the converter current in an axis created by a voltage in the other axis, are represented. These Bode plots are represented for the parameters in Table I, with the grid inductance equal to zero. R_d is a damping resistor in series with the filter capacitor, R_c is the converter series equivalent resistance and $R_{stransf}$ is the transformer series equivalent resistance With the classical voltage feed-forward, which uses a unity matrix for [FF], the cross-couplings in [LPAF] and $[D_{conv}]$ create a bad compensation at low frequencies, and the compensated system does not behave as a pure inductance equal to L_c, blue curve labeled ad *LCL FF clas*. If [FF] is equal to the matrix of Eq. 8, the effects of [LPAF] and $[D_{conv}]$ are completely canceled, and a pure inductance is obtained in the whole frequency range, up to the control Nyquist frequency (red curve: *LCL FF perf*). This option is not feasible, as the resulting transfer function has a greater number of zeros than

TABLE I
SYSTEM PARAMETERS

Parameter	Value	Parameter	Value
L_c	2.5 mH	R_d	3.5 Ω
L_{transf}	1.1 mH	F_{conm}	4 kHz
C_f	10 μF	F_{samp}	4 kHz
R_c	0.11 Ω	τ_{LPAF}	147 μs
$R_{stransf}$	0.07 Ω	S_{rated}	10 kW

poles. For this reason, Eq. 8 is approximated by a gain at a frequency of 0 Hz, obtaining a good decoupling at low frequencies as indicated in Fig. 7, by the curves labeled *LCL FF gain*.

With this voltage feed-forward, the variability at low frequencies is highly reduced and the CCD can be implemented for a pure inductance using the expressions in Eq. 4, with the emulated values been equal to the converter inductance value, even if the grid inductance is unknown. In Fig. 8 only two bode diagrams of the open loop transfer matrix are shown, as the system is symmetric, for two different short circuit ratios; 2 and 15 (SCR). In the upper graph, the diagonal terms of the open loop transfer matrix are plotted (I_{convd}/V_{contd}). In the lower one, the anti-diagonal terms (I_{convd}/V_{contq}). It can be concluded that the CCD provides a better decoupling between both axis than the conventional SFD with lower variability at low frequencies when the grid inductance varies. Particularly advantageous are the results for weak grids (SCR=2), where the proposed strategy allows to properly decouple both axis by more than 15 dB, while with the state feedback decoupling (SFD), the anti-diagonal terms are dominant at some frequencies, e.g. 0.4 Hz, and the dynamics cannot be decoupled. This is true up to frequencies around the resonance frequency, greater frequencies than the current controller bandwidth.

To sum up, the proposed decoupling strategy is based on an improved capacitor voltage feed-forward in the SRF to eliminate the *LCL* plant variability at low frequencies created by the unknown L_g. A decoupler, called CCD, is used to compensate the cross-coupling terms of the converter inductance, once that the variability at low frequencies is eliminated.

With this decoupling strategy, the design of the controller becomes simpler, as shown in the next subsection. Moreover, with the SFD stability problems may arise in high power converters and weak grids due to the stronger effects of the delays in the feedback compensation term.

C. Design of the controller

A PI controller is used in the SRF, as zero tracking error is achieved at the fundamental frequency (0 Hz in dq). In order to have at least a phase margin of 30 degrees for every grid inductance, considering a variation in the SCR from 2 to 400, a lead-lag compensator is also included. The PI has a k_p of 1.41

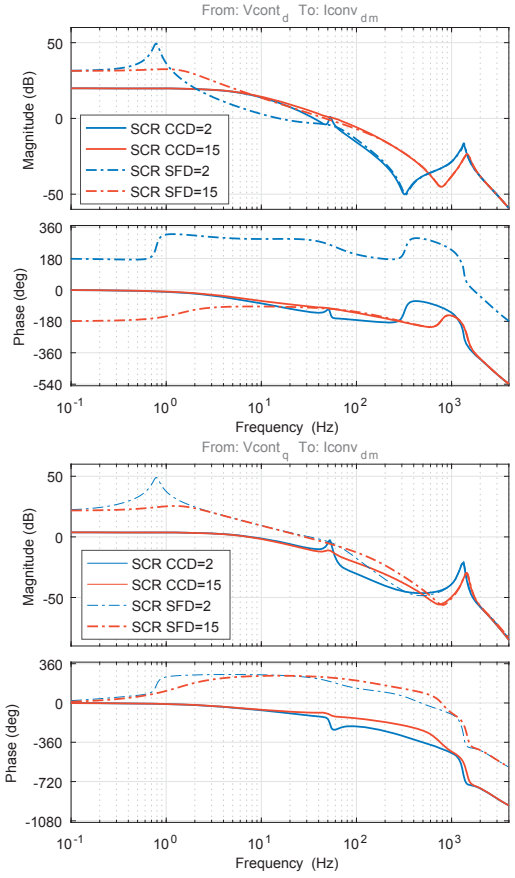

Fig. 8. Upper graph: Open loop frequency response of the d axis converter current to the d axis controller voltage ($I_{conv\ d}/V_{cont\ d}$) and lower graph: of the d axis converter current to the q axis controller voltage $I_{conv\ d}/V_{cont\ q}$, with the CCD (continuous) and SFD (discontinuous).

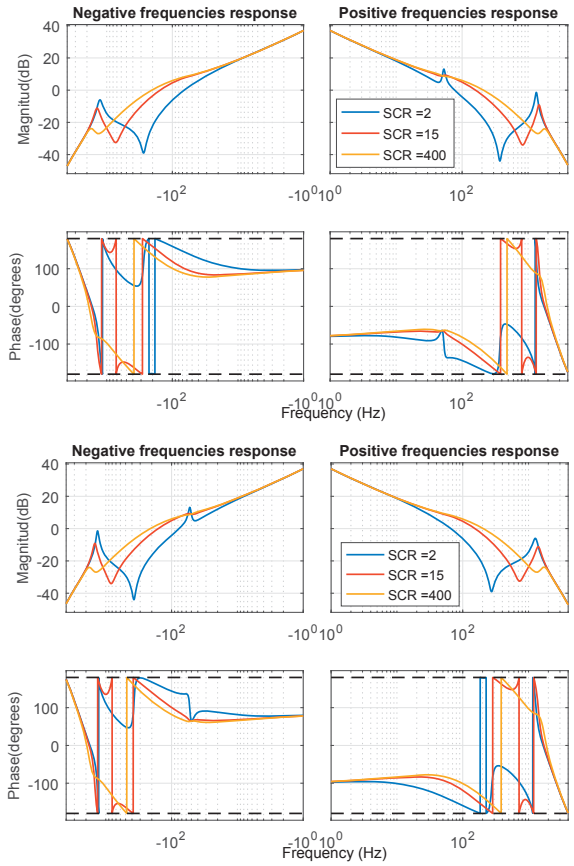

Fig. 9. Bode plots of the two eigenvalues of the open-loop transfer matrix, for positive and negative frequencies with the controller designed for the CCD strategy.

and a T_n of 32 ms, while the lead-lag is designed to introduce 30 degrees at 50 Hz. The stability margins achieved with this control structure are analyzed by means of the frequency response of the eigenvalues of the open loop transfer matrix [14], obtained from Fig. 6 by correlating $I_{conv\ dq\ f}(s)$ with $\varepsilon_{dq}(s)$. The frequency response of the two eigenvalues of the open loop transfer matrix is non-symmetric with respect to zero Hz, as complex values appear in the eigenvalues, for this reason, the Bode plots are represented at positive and negative frequencies in Fig. 9.

From Fig. 9 it can be concluded that at least a phase margin of 30 degrees is achieved within the controller bandwidth for the different SCR considered. As the open loop transfer matrix has no unstable poles and its eigenvalues have no crossings with -180 degrees with positive magnitude, the system is stable. The great magnitude at low frequencies and the guaranteed phase margin of 30 degrees, allows to conclude that a proper reference tracking is achieved. However, in a grid connected power converter, the rejection to grid disturbances is also important. In Fig. 6 the grid voltage is represented as a disturbance. To check the performance of the power converter against variations in the grid voltage, the closed loop transfer matrix correlating $I_{conv\ dq}$ with $V_{g\ dq}$ is obtained, representing the diagonal and anti-diagonal elements of this matrix in Fig. 10. Again, this matrix is symmetric, so only two components have to be represented. The fundamental component is seen as a dc component in dq, so it is almost eliminated. Moreover, for every frequency an attenuation of at least 11 dB is achieved.

To illustrate that with the proposed CCD the design of the controller becomes easier, in Fig. 11 the eigenvalues of the open-loop transfer matrix for the SFD are represented. This transfer matrix, as in the CCD case, also includes the controller. In this case, the transfer functions of the open loop transfer matrix have two unstable poles for every SCR, meaning that according to the Nyquist stability criteria, two encirclements of -1 are required in order to stabilize the system. This requirement is translated to the frequency response as 4 crossings with -180 degrees with a positive magnitude. This restriction has to be met, imposing a strong condition to the controller design. Moreover, the stability margins are reduced.

The last step to verify the performance of the proposed decoupling strategy, CCD, is the robustness face to parameter uncertainty. The CCD is based on the cancellation of the

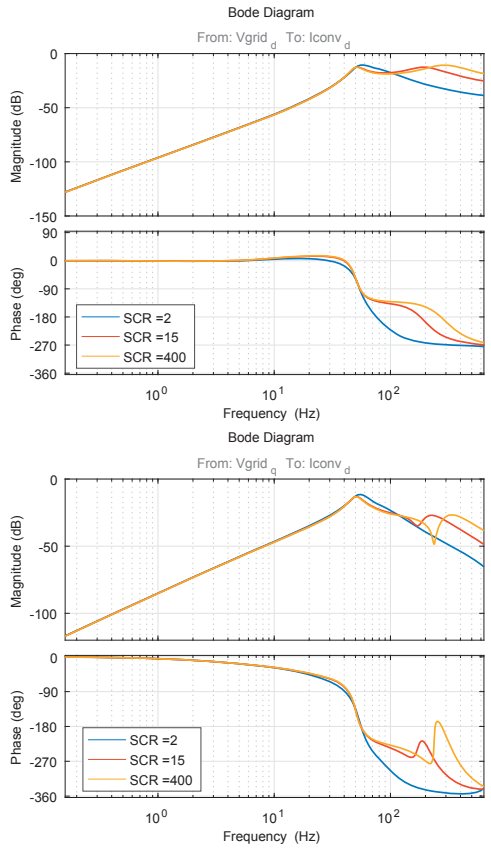

Fig. 10. Frequency response of the rejection to grid disturbances transfer matrix: in the upper graph $I_{conv\ d}/V_{g\ d}$ and in the lower graph $I_{conv\ d}/V_{g\ q}$.

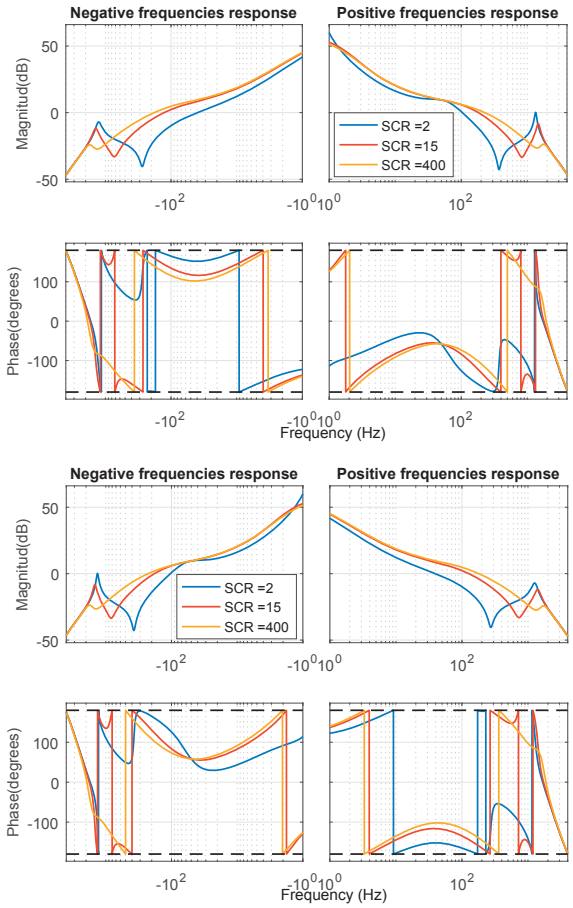

Fig. 11. Bode plots of the two eigenvalues of the open-loop transfer matrix, for positive and negative frequencies with the controller designed for the SFD strategy.

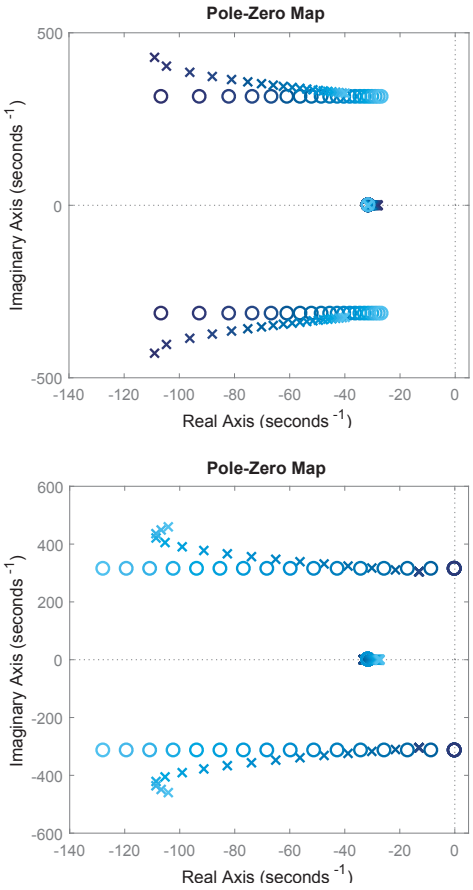

Fig. 12. Closed-loop pole evolution when the emulated inductance does not match the real converter inductance (upper graph) and when the emulated series resistance does not match the converter series resistance.

cross-coupling terms of the converter inductance once that the capacitor voltage feed-forward has been properly performed. For this reason, in the following, the effects of uncertainty on the parameters of the converter inductance, L_c and R_c, are analyzed. A $\pm 60\%$ variation in the converter inductance is introduced, while a $\pm 100\%$ variation is considered for the inductance series resistance. The greater range of variation in R_c is justified by the greater variations of this parameter with frequency, and because the resistance modeling the core losses is frequently unknown. In Fig. 12 in the upper graph, the variation of the slowest poles of the system is represented as L_e is modified with respect to the converter real inductance. In the lower graph the effect on the slowest poles of a modification in the emulated series resistance R_e, with respect to the real converter series resistance R_c, is represented. In both cases, the lighter blue poles represent an increase in the emulated parameter with respect to the real one, while a decrease is represented in darker blue. It can be concluded that despite the great variations considered in the emulated parameters the system does not become unstable, however, the response of the slowest poles can be penalized, reducing its damping. This happens when L_e is greater than L_c and when R_e is lower than R_c, so, in general, it is better to overestimate R_c and underestimate L_c.

IV. Validation of the Decoupling Strategy

To test the performance of the proposed decoupling strategy, simulations using Matlab SimPowerSystems toolbox are carried out. The simulated system is a 11 kW power converter. The modulation used is the space vector modulation, SVPWM7. The control loop is programmed in an S-Function, taking as inputs the measured converter currents and the capacitor voltage, and is executed once per switching period, performing symmetrical sampling. The output of the control function are the gate signals, implementing a dead time of 4 μs. A SCR of 2 is considered for the simulations. The system parameters are given in Table I, the same ones used for the stability analysis.

The effectiveness of the proposed decoupling strategy (CCD), is verified by comparing the step response of the CCD with the SFD and the system with no decoupling. This comparison is shown in Fig. 13, where the step response is plotted in the *dq* axis with the real current waveform. In the three cases, a step is introduced in the *d* axis at instant 0.4 s. It can be seen that with the CCD a better decoupling is achieved between *d* and *q*, as a result, a faster dynamic response is obtained that with the SFD, and way better if compared with the coupled system.

V. Conclusion

In this work a novel decoupling structure based on a MIMO cross-controller decoupler has been presented for a *LCL* filter controlled in the SRF. This strategy uses an improved capacitor voltage feed-forward in the SRF to eliminate the plant variability at low frequencies, created by the variable grid inductance. Once that this variability is eliminated, and the behavior of a pure inductance is obtained at low frequencies, a simple first order function is used to eliminate the cross-couplings, it is called cross-controller decoupler, CCD. With this decoupling strategy, a greater independence of the response of both orthogonal axis is achieved, specially in weak grids, improving its dynamic response. Moreover, with the CCD strategy, a higher bandwidth with greater stability margins can be achieved with a simple controller, resulting in a better dynamic response. Details on the controller design, robustness face to parameter uncertainties and rejection of grid disturbances are also provided.

Acknowledgment

The authors gratefully acknowledge INGETEAM POWER TECHNOLOGY for its financial and ongoing support

References

[1] "IEEE Application Guide for IEEE Std 1547, IEEE Standard for Interconnecting Distributed Resources With Electric Power Systems," IEEE Standard 1547.2-2008, 2009.

[2] M. Liserre, F. Blaabjerg, and S. Hansen, "Design and control of an lcl-filter-based three-phase active rectifier," *IEEE Transactions on industry applications*, vol. 41, no. 5, pp. 1281–1291, 2005.

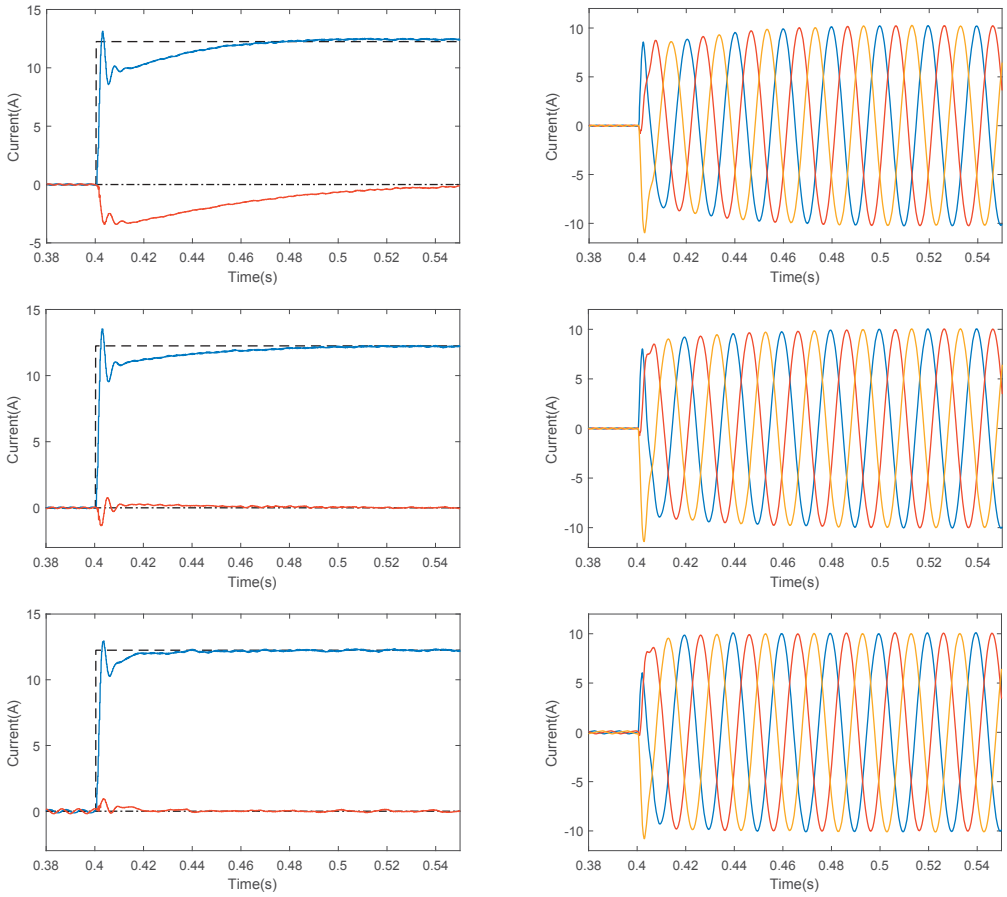

Fig. 13. Step response of the current control loop in *dq* axis and their real waveform: with no decoupling (upper graph), with SFD (middle graph) and the CCD (lower graph).

[3] X. Bao, F. Zhuo, Y. Tian, and P. Tan, "Simplified feedback linearization control of three-phase photovoltaic inverter with an lcl filter," *IEEE Transactions on Power Electronics*, vol. 28, no. 6, pp. 2739–2752, 2013.

[4] F. Blaabjerg, R. Teodorescu, M. Liserre, and A. V. Timbus, "Overview of control and grid synchronization for distributed power generation systems," *IEEE Transactions on industrial electronics*, vol. 53, no. 5, pp. 1398–1409, 2006.

[5] J. Dannehl, C. Wessels, and F. W. Fuchs, "Limitations of voltage-oriented pi current control of grid-connected pwm rectifiers with *lcl* filters," *IEEE Transactions on Industrial Electronics*, vol. 56, no. 2, pp. 380–388, 2009.

[6] F. Briz, M. W. Degner, and R. D. Lorenz, "Analysis and design of current regulators using complex vectors," *IEEE Transactions on Industry Applications*, vol. 36, no. 3, pp. 817–825, 2000.

[7] A. G. Yepes, A. Vidal, J. Malvar, O. López, and J. Doval-Gandoy, "Tuning method aimed at optimized settling time and overshoot for synchronous proportional-integral current control in electric machines," *IEEE Transactions on Power Electronics*, vol. 29, no. 6, pp. 3041–3054, 2014.

[8] B. Bahrani, S. Kenzelmann, and A. Rufer, "Multivariable-pi-based *dq* current control of voltage source converters with superior axis decoupling capability," *IEEE Transactions on Industrial Electronics*, vol. 58, no. 7, pp. 3016–3026, 2011.

[9] S. Zhou, J. Liu, L. Zhou, and Y. Zhang, "Dq current control of voltage source converters with a decoupling method based on preprocessed reference current feed-forward," *IEEE Transactions on Power Electronics*, vol. 32, no. 11, pp. 8904–8921, Nov 2017.

[10] J. L. Agorreta, M. Borrega, J. López, and L. Marroyo, "Modeling and control of n-paralleled grid-connected inverters with lcl filter coupled due to grid impedance in pv plants," *IEEE Transactions on Power Electronics*, vol. 26, no. 3, pp. 770–785, 2011.

[11] J. Samanes and E. Gubía, "Sensorless active damping strategy for parallel interleaved voltage source power converters with lcl filter," in *Applied Power Electronics Conference and Exposition (APEC), 2017 IEEE*. IEEE, 2017, pp. 3632–3639.

[12] D. N. Zmood, D. G. Holmes, and G. H. Bode, "Frequency-domain analysis of three-phase linear current regulators," *IEEE Transactions on Industry Applications*, vol. 37, no. 2, pp. 601–610, 2001.

[13] X. Li, J. Fang, Y. Tang, X. Wu, and Y. Geng, "Capacitor-voltage feedforward with full delay compensation to improve weak grids adaptability of lcl-filtered grid-connected converters for distributed generation systems," *IEEE Transactions on Power Electronics*, vol. 33, no. 1, pp. 749–764, 2018.

[14] L. Harnefors, "Modeling of three-phase dynamic systems using complex transfer functions and transfer matrices," *IEEE Transactions on Industrial Electronics*, vol. 54, no. 4, pp. 2239–2248, 2007.